Journal of Catalysis 443 (2025) 115960

Contents lists available at ScienceDirect

Journal of Catalysis

journal homepage: www.elsevier.com/locate/jcat

Research article

The role of nanoporosity in oxygen reduction reaction under elevated mass transport: Porous vs core-shell

Primož Jovanovič [a,*], Armin Hrnjić [a,b], Luka Pavko [a], Martin Šala [c], Francisco-Ruiz Zepeda [a], Marjan Bele [a], Nejc Hodnik [a,b]

[a] Department of Materials Chemistry, National Institute of Chemistry, Hajdrihova 19, SI-1000 Ljubljana, Slovenia
[b] University of Nova Gorica, Vipavska 13, SI-5000 Nova Gorica, Slovenia
[c] Department of Analytical Chemistry, National Institute of Chemistry, Hajdrihova 19, 1000 Ljubljana, Slovenia

A B S T R A C T

Reliable assessment of electrocatalytic performance of novel materials to determine the oxygen reduction (ORR) activity plays a pivotal role in systematic-driven design of tailored composites. Unfortunately rotating disc electrode technique, typically employed for this purpose, is incapable to accurately predict the behaviour of promising candidates in membrane electrode assemblies (MEAs) which are finally used in fuel cells. Instead, miniature electrochemical setups based on floating electrode, which mimics MEA's three-phase boundary active sites, has recently been recognized as an adequate diagnostics substitute. Compared to conventional RDE the working electrode operating under floating regime makes the acquisition of catalysts' behaviour at low potentials easily achieved without being limited by the solubility and/or mass transport of O_2 in aqueous electrolyte. Accordingly, the present study employs a modified version of the floating electrode methodology (MFE) to accurately investigate the effect of electrocatalyst nanostructure on high-current density ORR performance. Two morphologically distinct platinum-based de-alloyed nanoparticle samples—porous and non-porous core–shell analogues—are compared. The analysis reveals that at the high current density region (< 0.8 V vs RHE) porous nanoparticles demonstrate significantly worse ORR specific activities in comparison to core–shell analogues. On the other hand, the performance is reversed at low current densities (> 0.8 V vs RHE) supporting the results from the RDE analysis. The observed trend is attributed to a reduction in the utilization of active surface area in nanoporous catalysts with increasing overpotential.

1. Introduction

Proton Exchange Membrane Fuel Cells (PEMFCs) are among the most promising candidates likely to change the landscape of future energy conversion, since they provide independence from fossil fuels without heavy environmental toll. On the pathway to their broader implementation, several restrictions have to be addressed, with the most vital one being the performance and the cost-effective utilization of electrocatalysts. During past decades we witnessed a very fast development of novel electrocatalysts with extremely improved activity [1,2]. Primarily, the focus has been on thorough investigation of alloying and shape control of platinum containing catalysts with a plethora of variants markedly surpassing required thresholds [3–7]. Within core–shell nanoparticles (i.e., platinum enriched shell and non-noble metal enriched alloy core) have received enormous attention. Here experimental and theoretical investigations suggested that core–shell are beneficial for ORR kinetics because of the modified d-band center of surface Pt atoms caused by the underneath alloying effect [8–10]. Typically, a core–shell architecture is evolved during de-alloying when the selective etching removes the less-noble transition metals and naturally forms a Pt passivated surface [11]. Equally attractive have been porous bimetallic composites where confinement effect induced within the pores has been demonstrated beneficial for ORR [12,13]. In this case the same preparative strategy can be employed provided that parting limits such as size, composition and the critical potential of bimetallic nanoparticles are met during de-alloying [14,15]. Although advancements in the ORR performance on the laboratory scale are impressive for both, core–shell as well as nanoporous catalysts, there is no guarantee that the trend will reflect under real device regime. There the electrochemical conditions and mass transport environment are significantly different in comparison to conventional rotating disc electrode (RDE) measurements. Even though a rapid characterization is possible the RDE can only measure the kinetic response in a narrow overpotential range limited to potentials above 0.8 V vs RHE [16]. A membrane electrode assembly (MEA) on the other hand operates under orders of magnitude larger current densities and much wider potential window (0.6–0.8 V) both of which are inaccessible to RDE [17–20]. Hence the wide gap between RDE predictions and MEA reality

* Corresponding author.
E-mail address: primoz.jovanovic@ki.si (P. Jovanovič).

https://doi.org/10.1016/j.jcat.2025.115960
Received 28 November 2024; Accepted 9 January 2025
Available online 11 January 2025

[4,21–26]. Indeed there is a strong incentive for electrochemical techniques enabling accurate characterization at high current densities already at an early stage of catalyst development where only small amounts of catalyst are available. Indeed, few research groups have engaged in this direction implementing mainly two types of approaches, i.e., the so-called floating electrode technique (FET)[19,27–31] and the gas diffusion electrode (GDE).[23,32] In the FET case the catalyst ink is implemented on, porous Au coated polycarbonate membrane (thickness of ~12 μm) floating on the electrolyte and oxygen is supplied to the catalyst through the membrane pores directly from the gas phase. To perform electrochemical measurements extremely small quantities of catalyst powder are needed 1–15 $\mu g_{Pt} cm^{-2}$) [28,30,31]. In a typical GDE on the other hand the ink is spray-coated or inkjet-printed on gas diffusion layer and oxygen is supplied to the catalyst via convective flow field [23]. Here larger catalyst amounts are necessary (loadings of 0.02–0.4 $mg_{Pt} cm^{-2}$). Regardless, both setups allow ORR activity to be determined in a wide potential window without correcting for the mass transport. Recently, the floating electrode concept has been adopted by our group utilizing carbon coated transmission electron microscopy (TEM) grids as electrode substrates (referred from hereon as the modified floating electrode, MFE). Even though in this case the accessible current density range is narrower than in the case of GDE-based setups, [32] the MFE still provides access to significantly larger current densities than RDE (similar to the FET methodology). Also here, very small amounts of catalyst are needed (3–22 $\mu g_{Pt} cm^{-2}$) [33].

Within this study, we exploit MFE to investigate omnipresent ORR electrocatalysts, namely dealloyed Pt nanoparticles. The focus is placed on comparative analysis of a core–shell and a nanoporous analogue, however under wide potential range (i.e., current densities) inaccessible to conventional RDE methodology. We demonstrate that at low current densities RDE trends are retained also under MFE conditions. However, evidence on declining ORR performance trend when nanoparticles' structure goes from nanoporous to core–shell type is provided.

2. Experimental

2.1. Synthesis

The goal was to compare electrochemical performance of analogues with or without porous structure. Accordingly, Pt-Cu/C nanoparticles with adequate size and composition to evolve porosity upon electrochemical de-alloying were synthesized (referred from hereon as np-Pt-Cu). The corresponding ORR performance was compared to commercial bulk platinum and non-porous alloyed analogues (i.e., core–shell type).

Pt-Cu synthesis: We emphasize that the synthesis of Pt-Cu composite investigated herein is described in detail in our recent publication [17]. Briefly, the synthesis consists of two vital steps, the first being annealing of a Cu salt precursor together with gelatine and carbon black to obtain Cu particles in a porous carbon matrix. In the second part, the Cu from the composite is partly galvanically displaced by a Pt precursor (K_2PtCl_4) and annealed for the second time. A detailed, point by point description of the synthesis procedure is given in Supporting Information (section S1).

Commercial core–shell alloys: Pt-Co/C, Pt-Fe/C and Pt-Cu/C commercial composites (purchased at Fuel Cell Store, USA) were included in comparison. Based on supplier's description the samples consist of 20 wt% metal loading (Pt:M 1:1 atomic ratio) supported on Vulcan XC-72 carbon with an average metallic particle size of 2–3 nm [34]. ICP-OES digestion results of electrocatalysts in the as-purchased state confirmed the stated 1:1 atomic ratio of Pt to M and a total metal loading (Pt + M) of approximately 20 wt% (see Table 1).

Commercial bulk platinum: For the purpose of comparative ORR analysis a commercial sample of platinum nanoparticles dispersed on carbon support (TEC10E50E-HT from Tanaka Kikinzoku Kogyo, Japan) was analysed as well.

2.2. Structural characterization

Transmission electron microscopy: Electron microscopy was performed in a Cs corrected microscope CF-ARM Jeol operated at 200 kV and 80 kV. Annular dark field (ADF) images were taken with 45–180 mrad and with 68 and 280 mrad for inner and outer semi angles. Convergence angle was about 25 mrads.

ICP-OES characterization: All reagents used were of analytical grade or better. For sample dilution and preparation of standards, ultrapure water (Milli-Q, Millipore) and ultrapure acids (HNO_3 and HCl, Merck-Suprapur) were used. Standards were prepared in-house by dilution of certified, traceable, inductively coupled plasma (ICP)-grade single-element standards (Merck CertiPUR). A Varian 715-ES ICP optical emission spectrometer was used. Prior to ICP-OES analysis, each sample was weighed (approximately 10 mg) and digested using a microwave-assisted digestion system (CEM MDS-2000) in a solution of 6 mL HCl and 2 mL HNO_3. The digested samples were cooled to RT and then diluted with 2 %v/v HNO_3 until their concentration was within the desired concentration range. After the digestion procedure, samples were centrifuged to yield clear solutions that were used in subsequent analysis.

2.3. Electrochemical measurements

Modified floating electrode (MFE): For conducting ORR measurements under elevated mass transport of O_2 our recently introduced modified floating electrode apparatus was employed [33]. In this case the working electrode operates in the so-called floating mode meaning that that the electrode is not dipped in the electrolyte solution, as is in the case of TF-RDE, but is instead placed on its surface. The WE compartment is made of two-piece Teflon housing, which was assembled with PEEK-based screws. Between the housing elements the following elements are inserted: a metallic spring, two metallic cones, a gas diffusion layer (GDL, 280 μm thickness) with 40 % Teflon weight wet proofing (Toray Carbon Paper 090, Fuel CellStore) and gold TEM grid working electrode (Agar Scientific, Holey Carbon Films on 300 Mesh Gold). The TEM grid was inserted below the GDL, whereas the spring and two metallic cones were pressed above the GDL (see Fig. 1). We note that the Teflon in GDL gave the carbon material a hydrophobic property, which prevented the electrolyte from penetrating and creeping to the metallic cone and spring contacts hence preventing their damage or even dissolution and thus potentially impacting electrochemical measurements. The GDE, therefore, served as a spacer to separate the working electrode from the

Table 1
Summary of investigated samples.

Catalyst	Average particle size [TEM/ nm]	ORR_{spec}@0.9 V RDE [mA/cm^2]	$ECSA_{CO}$ [m^2/g_{Pt}]	Pt loading [wt. %]	Ratio (Pt:M) [at. %] *
Pt/C	4.8[16,35–37]	0.29	44	50.6	/
np-Pt-Cu	18.1	2.35	43	20.27	26.49: 73.51
Pt-Fe/C[38]	2.5	1.32	68	17.84	50.23: 49.77
Pt-Co/C[38]	3.5	1.17	67	18.08	50.52: 49.48
Pt-Cu/C[38]	2.3	1.24	72	14.24	50.37: 49.63

* Chemical composition in the as prepared state.

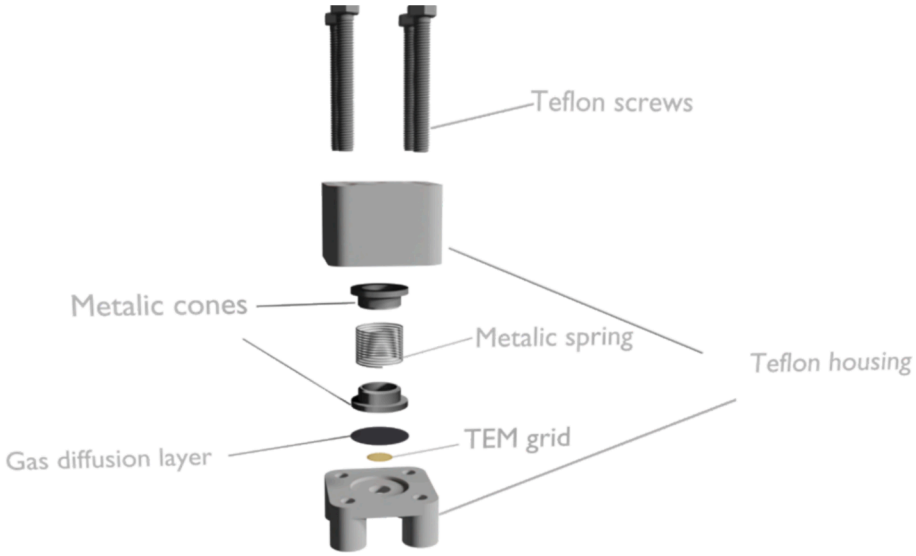

Fig. 1. Schematic presentation of the MFE setup.

metallic cones and spring. All three served as an electrical contact for the gold TEM grid working electrode. Gas purging tube was connected to one of the holes of the Teflon housing via Teflon tubing (see Fig. 1).

Catalyts' ink composition consisted of the following ratios: catalyst mass (mg) vs. solvent volume (mL) 5:3. Solvent composition in terms of volume fractions was set as follows: (75 % propane-2-ol, 25 % mili Q water and 1.33 % Nafion® (ElectroChem, 5 wt% aqueous solution). Inks were ultrasonicated (Ultrasound bath Iskra Sonis 4) for 30 min prior to dropcasting. Catalyst ink was deposited on TEM grid by drop casting with syringe (Hamilton). Catalyst film was dried on a heating stage. Dropcasting was performed on Au side of the grid which was later exposed to the electrolyte during electrochemical measurements. A two-compartment (H-type), Teflon based 10 ml electrochemical cell was used. Platinum mesh counter electrode (GoodFellow 50 × 50 mm) and reversible hydrogen reference electrode (HydroFlex®) were both placed in the same compartment. In a separate compartment, modified floating electrode housing was placed. The two compartments were separated by a Nafion membrane (Nafion 117, FuelCellStore). 4 M perchloric acid ($HClO_4$, Merck, Suprapur, 70 %, diluted by Milli-Q, 18.2 MΩ cm) was used as a working electrolyte as typically used in similar electrode configurations to reduce the ionic resistance of the electrolyte [19,31]. The following electrochemical protocol was performed. Initially, a typical electrochemical pre-treatment was performed in order to obtain a stable cyclic voltammogram (CV). This consisted of potentiodynamic perturbation by cycling the potential between 0.05–1.1 V vs RHE (200 cycles, 300 mV s^{-1}) under the nitrogen atmosphere. Afterward the electrolyte was exchanged with a fresh one, nitrogen was replaced by oxygen gas and ORR polarization curves with Ohmic drop compensation were recorded 20 mV s^{-1}. We emphasize that for each individual sample the ORR analysis was conducted in the loading independent ORR_{spec} regime (SI sections S4) ensuring a comparison of intrinsic ORR performances (i.e., without additional mass transport effects).[30,33] iR resistance between the working and reference electrode was measured using the high-frequency intercept of an impedance scan for each electrode (measured at open circuit potential). Ohmic drop compensation (85 %) was applied during electrochemical experiments via positive feedback mode. Hydrogen under potential deposition (HUPD) was used to determine the Pt surface area via integrating the HUPD feature under a fast potentiodynamic experiment (300 mV s^{-1}).

3. Results

Scanning Transmission Electron Microscopy imaging of np-Pt-Cu and Pt-Fe/C: Nanoparticles corresponding to np-Pt-Cu and Pt-Fe/C, both collected after electrochemical pre-treatment, were analyzed under the scanning transmission electron microscope (STM) to address the relationship between porosity to size. As can be seen in Fig. 2, np-Pt-Cu analogue shows a bimodal size distribution, one around 25 nm, and a second distribution below 10 nm. It can be observed that some of the large particles display signs of porosity, ranging from mild to severe etching. In contrast, in the case of Pt-Fe the particles show a size distribution around 4 nm, and manifest significantly less formation of pores as expected based on size-dependency of porosity evolution [15].

ORR comparison Pt/C vs *np-Pt-Cu:* Initial electrochemical measurements focused on comparative analysis of ORR performances of the homemade np-Pt-Cu and commercial bulk platinum sample (Pt/C) measured under conventional thin film rotating disc electrode (TF-RDE) configuration (Fig. 3**a** and Table 1). The TF-RDE trends are in accordance with the superior performance of dealloyed catalysts over bulk platinum demonstrated in numerous other reports [39–41]. Note, however, that under TF-RDE conditions the ORR kinetics is accessible only within a very narrow potential range preventing one from obtaining reliable performance trends outside this region. Therefore, even though de-alloyed porous analogues manifest promising predispositions this doe not ensure their performance is retained under a more realistic regime (i.e. higher current densities). Notably, apart from some scarce MEA investigation [21,42] there are no such studies enabling a critical perspective on porosity. Therefore our further investigation exploited the MFE setup. According to the obtained trends, the np-Pt-Cu analogue indeed retains better ORR performance in the entire potential window (Fig. 3**b**). This suggests that behaviour at low overpotentials (low current density regime) might be a reliable prediction for the trends at high overpotentials (high current density regime). Roughly similar trends were also obtained recently for the case of dealloyed Pt-Co composites by the original FET methodology [30]. However in that particular case non-porous analogues (i.e. core–shell type) were included in the comparison which might present an important distinction to porosity. In particular, apart from typical electronic effects at play in alloyed nanoparticles such as (ligand and/or strain [9,43,44]) porous analogues on the other hand additionally manifest the geometric effect (nano-confinement) [42,45–47] Hence, we expanded our investigation towards comparative electrochemical analysis of a porous and a core–shell analogue.

ORR comparison Pt-Fe/C vs *np-Pt-Cu:* Accordingly, a commercial Pt-Fe sample (i.e., core–shell type, Fig. 2**b** and Table 1) was evaluated via MFE configuration and compared to np-Pt-Cu analogue i.e. a sample

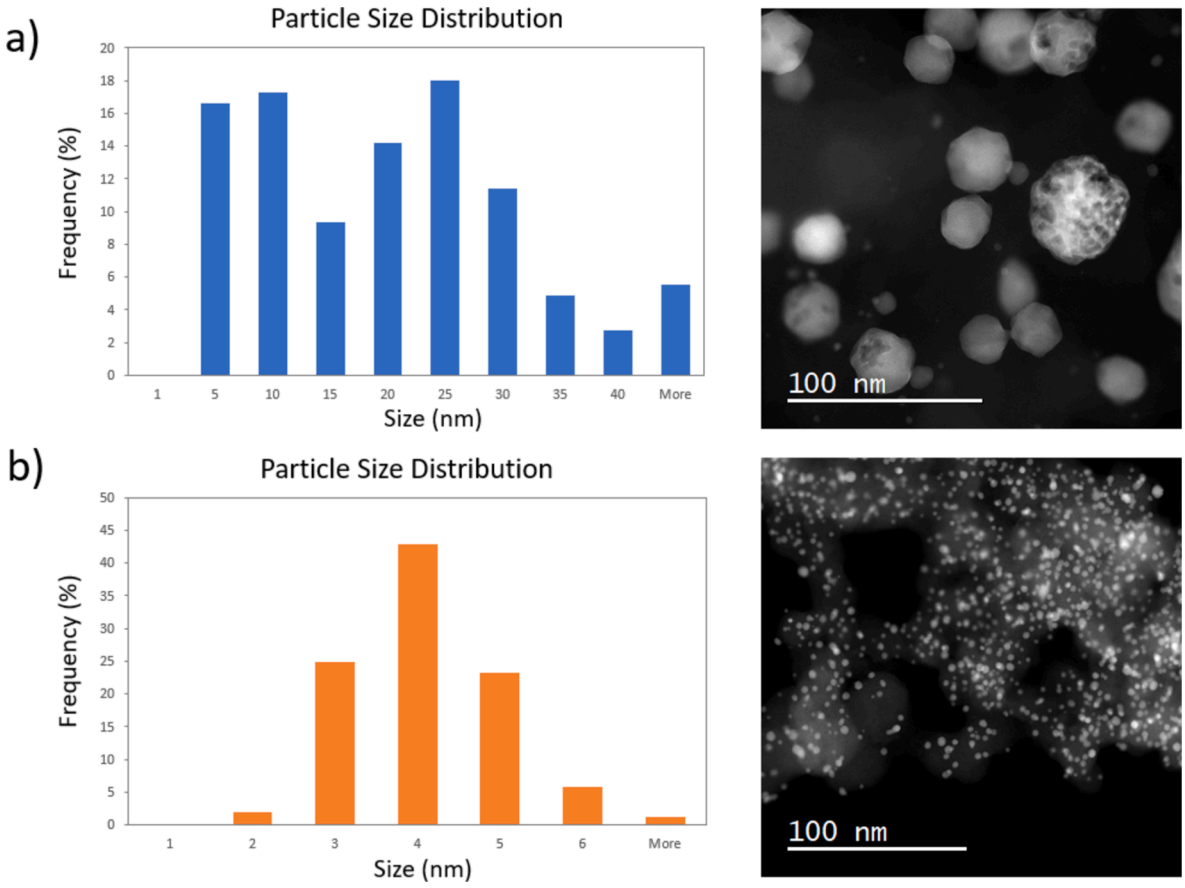

Fig. 2. Particle size distributions and representative ADF images of **a)** np-Pt-Cu and **b)** Pt-Fe after electrochemical pre-treatment.

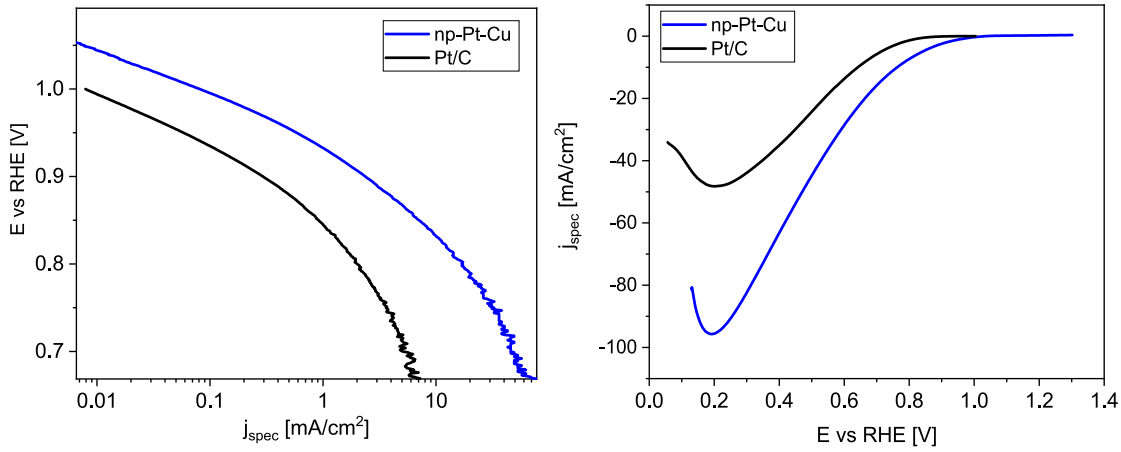

Fig. 3. ORR polarization curves for Pt/C and np-Pt-Cu samples. **a)** TF-RDE comparison (20 mV/s, 0.1 M $HClO_4$) presented as Tafel plots. **b)** Background corrected ORR polarization curves (anodic scan shown) obtained via MFE setup (20 mV/s, 4 M $HClO_4$).

with a large population of porous particles (Fig. 2**a**). Interestingly, the ORR_{spec} performance can be divided into two opposite trends depending on the potential region as follows. Initially, in the low current density region, the np-Pt-Cu sample outperforms the core–shell analogue (Fig. 4**a**) which is in accordance with predictions from the TF-RDE measurements (Table 1). However, when approaching lower potentials (i.e., higher current densities) the two polarization curves diverge and the core–shell sample substantially outperforms the porous analogue (Fig. 4**a**,**b**).

4. Discussion

Overall, the discrepancy between the low and high current density trends suggests two limiting scenarios. Namely, ORR is susceptible to mass transport limitations (i.e. a non-intrinsic effect) and/or the reaction kinetics at low potentials is altered in favour of the core–shell architecture (i.e. an intrinsic effect). Initially, we address the mass transport limitation where, capitalizing from MEA studies, the most obvious explanation could rely on the local O_2 resistance, R_{O2}^{Pt}, which describes the O_2 interfacial transport through the ionomer film towards Pt surface. As shown recently ORR performance at high current densities

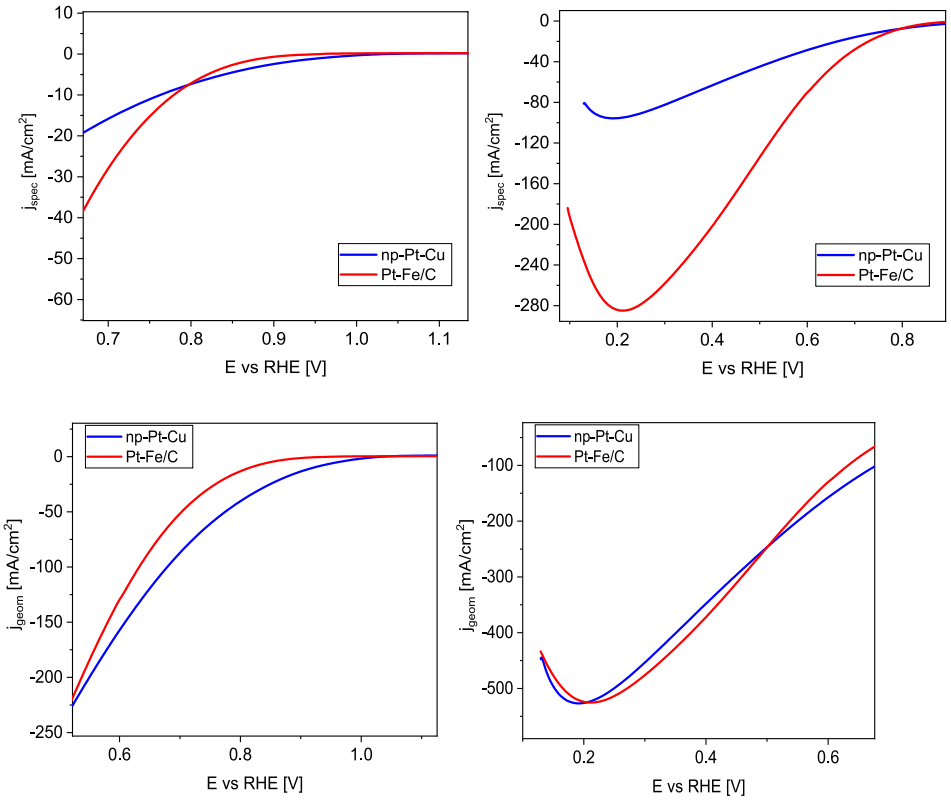

Fig. 4. Background corrected ORR polarization curves for np-Pt-Cu and Pt-Fe analogue (anodic scan shown) obtained via MFE setup (20 mV/s, 4 M $HClO_4$) demonstrated as ORR_{spec} (a-b) or ORR_{geo} (c-d).

is hypothesized to be predominantly governed by R^{Pt}_{O2}. However, one of the strong arguments against its influence in our case is that it has been put forward based on MEA-based measurements [25,48–52] and hypothesized to play an important role under much higher current densities ($>$ 1 Acm^{-2}_{geo}) than reached in our work ($\leq$ 500 $mAcm^{-2}_{geo}$). Furthermore, studies involving the R^{Pt}_{O2} assumed an exponential increase of ORR current also in the oxide-free region (low potentials) ascribing observed deviations to R^{Pt}_{O2}. However as shown in recent FET studies two other factors should be, at least, equally relevant. Firstly, the blocking of Pt surface with ORR intermediates in the oxide-free region (low potentials) also leads to a decline from the exponential behaviour [30,53]. The second factor is the preferential adsorption of negatively charged sulfonate groups from the ionomer where the unexpectedly ionomer-free electrode (i.e. with more Pt-free sites) showed only slightly better ORR_{spec} from the ionomer-coated electrode (i.e. with less Pt free sites) in the oxide-free region (low potentials, 0.1–0.4 V) [28]. Notably in the referenced FET studies current densities in the range of 1 Acm^{-2}_{geo} were reached therefore closely approaching the MEA regime. This further increases the validity/credibility that R^{Pt}_{O2}, might not be the predominant performance descriptor at low potentials. On the other hand in the oxide-covered region (higher potentials) the Nafion-coated electrode manifested better performance. The authors suggested that sulfonate groups lower the activation energy for ORR, however this effect attenuates in the oxide-free region (low potentials) where the characteristics of more free sites (the Nafion-free electrode) becomes the prevailing factor [28]. Similarly, we investigated the effect of ionomer content for the Pt/C analogue. Accordingly, Nafion-free electrode manifests only slightly better performance at low potentials (Fig. 5**b**) but worse at high potentials (Fig. 5**a**) in comparison to Nafion-coated analogue in accordance with the results from the FET [28]. We note again that if R^{Pt}_{O2} were to limit the reaction in the MFE configuration the Nafion-coated analogue should manifest worse ORR_{spec} performance at

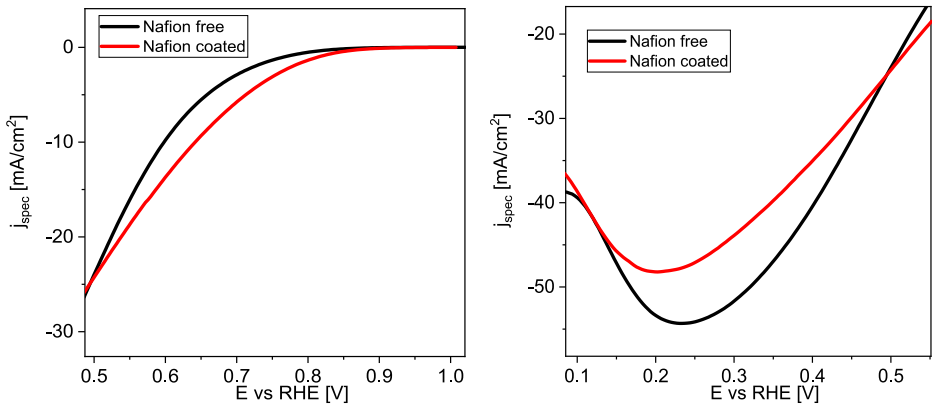

Fig. 5. ORR_{spec} polarization curve for Nafion-free and Nafion-coated Pt/C catalyst (4 M $HClO_4$, 20 mV/s, anodic scan shown). Ionomer/carbon ratio = 0.8 mg/mg.

low potentials (high current densities). Therefore the performance alterations for np-Pt-Cu and Pt-Fe analogues should be ascribed to intrinsic (morphological) differences. On the other hand, R_{O2}^{Pt} is influenced by dispersion of the catalyst (i.e. inter-particle distance). Note that the two analogues have similar Pt mass loading (Table 1) but since np-Pt-Cu has larger particles the inter-particle distance is larger for the latter. This could account for its lower ORR_{spec} at high overpotentials (Fig. 4**b**). However, FET measurements of Pt/C analogues with different inter-particle distance disclosed that ORR_{spec} is mainly governed by particle morphology. In particular, composites with fixed platinum-to-carbon ratio but unique particle size demonstrated the trend of increased ORR_{spec} with the particle size [30]. Note that if the inter-particle distance had signigicant effect the ORR_{spec} should decline with the particle size since larger particles are are more separated.

Overall, we suggest an alternative explanation for the obtained ORR_{spec} trends where we argue that for the case of nanoporous catalysts the postulate that ECSA is completely utilized may not hold for the entire ORR potential window. In other words, *"ORR participating ECSA"* is possibly a function of the potential and decreases with increasing the ORR overpotential. Under such particular conditions, the reaction may occur only at the outermost geometric surface excluding the participation of pores in the reaction. Therefore the effective area may not always be the same as the one accessible to the electrolyte (i.e. from which the HUPD or CO stripping charge is used to calculate the active surface area). More specifically, in the high-overpotential regime, the statistical probability for incoming O_2 molecules to undergo ORR is high (~ 100 %) for both, the porous and non-porous surfaces. The reaction proceeds at the outer electrode's surface meaning the effective surface area is the same for both analogues. In contrast, in the low-overpotential regime (i.e., low reaction driving force) the probability of O_2 molecules to react on the entire electrochemically active surface area is much higher. This means that the confinement effect of porous electrodes can come into play, hence the higher ORR activity for the np-Pt-Cu analogue (Fig. 4**a**). The hypothesis on similar effective surface area at high overpotentials and dissimilar effective surface area at low overpotentials can be further verified by comparing ORR performance presented as geometric current densities (ORR_{geom}) for the two analogues. If our hypothesis is valid the difference in ORR_{geom} should be gradually decreasing with increasing the overpotential. When normalized per geometric surface area much smaller differences as in ORR_{spec} should be obtained whereas the ORR_{geom} at low overpotenitals should still significantly differentiate. Indeed the corresponding comparison reveals that this seems to be the case (Fig. 4**c,d**). We note that similar behaviour was previously observed in RDE measurements from where the same rationale was used to explain ORR trends [12]. However, we emphasize that there the probed potential range was limited (due to obvious limitations of RDE configuration) to ~ 0.8 V vs RHE whereas in the present case, owing to the unique configuration of MFE apparatus, the potential window can be considerably widened (~ 0.05 V vs RHE). To corroborate this even further, an analogous comparative analysis was performed by considering two additional core–shell samples, i.e., a Pt-Co analogue (see section S4 in Supplementary) and a Pt-Cu analogue (see section S4 in Supplementary). Accordingly, a similar potential-dependant trend as in the initial comparison of np-Pt-Cu and Pt-Fe was obtained (see sections S7 and S8 in Supplementary).

5. Conclusion

The present study investigates two limiting examples of nanoparticulate morphology, namely a porous and a non-porous one focusing on the corresponding ORR performance. Accordingly, we performed a comparative ORR analysis of two typical platinum-based de-alloyed catalysts, namely a core–shell and a nanoporous analogue. For the purpose of the study, our unique floating-type electrode diagnostics was employed which, compared to a conventional TF-RDE method, enabled ORR measurements to be conducted under elevated mass transport of O_2. In this way, the potential window of interest was significantly expanded. Accordingly, the analysis disclosed an evident anomaly. Namely, at low overpotentials the nanoporous analogue shows superior performance, which is in accordance with TF-RDE measurements. However, at high ORR overpotentials, the core–shell sample significantly outperforms the nanoporous analogue. To elaborate on this discrepancy we propose that in nanoporous architecture "ORR participating ECSA" is probably a function of the potential and decreases with increasing the ORR overpotential similarly to what was originally suggested by Erlebacher's TF-RDE analysis [13,54]. Under such conditions, a portion of the catalyst's surface area is not electrochemically active due to transport limitation into the pores. The impact of the present study can be divided into two segments. Firstly, as demonstrated herein such insight is inaccessible with conventional RDE methodology with limited potential window and therefore highlights the importance of employing electrodes with elevated mass transport capabilities already at the initial stage of catalyst evaluation. Secondly, our findings imply that a porous architecture needs to be carefully designed if the potentially beneficial effect of nanoconfinement is to be exploited to its full potential. One of the viable means to exploit is the usage of pore-filling additives enabling increased O_2 solubility. One class example are specific ionic liquids (ILs). In conjunction with confined space, the latter indeed demonstrate improved ORR performance due to increased attempt frequency in comparison to blank composite as demonstrated in pioneered studies by Erlebacher's group [13,54]. However, these composites are typically characterized in a limited potential window via TF-RDE, hence the understanding of IL additives is still in the preliminary stage especially when it comes to behaviour under a high current density regime. Therefore key properties of this secondary phase still need to be elucidated in order to increase the composite catalyst's overall activity.

CRediT authorship contribution statement

Primož Jovanovič: Conceptualization, Formal analysis, Funding acquisition, Investigation, Methodology, Supervision, Validation, Writing – original draft, Writing – review & editing. **Armin Hrnjić:** Investigation. **Luka Pavko:** Investigation. **Martin Šala:** Investigation. **Francisco-Ruiz Zepeda:** Investigation, Methodology, Writing – original draft. **Marjan Bele:** Investigation, Methodology. **Nejc Hodnik:** Funding acquisition, Supervision.

Declaration of competing interest

The authors declare that they have no known competing financial interests or personal relationships that could have appeared to influence the work reported in this paper.

Acknowledgements

The authors would like to acknowledge the Slovenian Research and Innovation Agency (ARIS) programs P2–0393, P1–0034 and I0–0003; the projects N2–0155, N2–0257, J2-3041, J7–4637, J7–50227 and MN-0007-104; European Research Council (ERC) Starting Grant 123STABLE (grant agreement ID: 852208). The authors acknowledge partial support from the Republic of Slovenia, Ministry of Higher Education, Science and Innovation, and from the European Union – NextGenerationEU in the framework of the project HyBReED, that is part of the Slovenian Recovery and Resilience Plan. Views and opinions expressed are however those of the authors only and do not necessarily reflect those of the Republic of Slovenia, Ministry of Higher Education, the European Union or the European Commission. Neither the the Republic of Slovenia, Ministry of Higher Education, Science and Innovation, European Union nor the European Commission can be held responsible for them.

Appendix A. Supplementary material

Supplementary data to this article can be found online at https://doi.org/10.1016/j.jcat.2025.115960.

Data availability

Data will be made available on request.

References

[1] I. Katsounaros, S. Cherevko, A.R. Zeradjanin, K.J.J. Mayrhofer, Oxygen electrochemistry as a cornerstone for sustainable energy conversion, Angew. Chemie Int. Ed. 53 (2014) 102–121, https://doi.org/10.1002/anie.201306588.

[2] N.M. Markovic, Electrocatalysis: Interfacing electrochemistry, Nat. Mater. 12 (2013) 101–102, https://doi.org/10.1038/nmat3554.

[3] O. Gröger, H.A. Gasteiger, J.-P. Suchsland, Review—electromobility: batteries or fuel cells? J. Electrochem. Soc. 162 (2015) A2605–A2622, https://doi.org/10.1149/2.0211514jes.

[4] M.K. Debe, Electrocatalyst approaches and challenges for automotive fuel cells, Nature 486 (2012) 43–51, https://doi.org/10.1038/nature11115.

[5] B. Ifan, E. Lester, J. Rossmeisl, I. Chorkendorff, Toward Sustainable Fuel Cells 354 (2016) 1378–1380.

[6] K. Kodama, T. Nagai, A. Kuwaki, R. Jinnouchi, Y. Morimoto, Challenges in applying highly active Pt-based nanostructured catalysts for oxygen reduction reactions to fuel cell vehicles, Nat. Nanotechnol. (2021), https://doi.org/10.1038/s41565-020-00824-w.

[7] S.P.N. Nanopolyhedra, J. Zhang, H. Yang, J. Fang, S. Zou, Synthesis and Oxygen Reduction Activity of, (2010) 638–644. DOI: 10.1021/nl903717z.

[8] C. Wang, M. Chi, D. Li, D. Strmcnik, D. van der Vliet, G. Wang, V. Komanicky, K. Chang, A.P. Paulikas, D. Tripkovic, J. Pearson, K.L. More, N.M. Markovic, V. R. Stamenkovic, D. Van Der Vliet, Design and synthesis of bimetallic electrocatalyst with multilayered Pt-skin surfaces, J. Am. Chem. Soc. 133 (2011) 14396–14403, https://doi.org/10.1021/ja2047655.

[9] P. Strasser, S. Koh, T. Anniyev, J. Greeley, K. More, C. Yu, Z. Liu, S. Kaya, D. Nordlund, H. Ogasawara, M.F. Toney, A. Nilsson, Lattice-strain control of the activity in dealloyed core-shell fuel cell catalysts, Nat. Chem. 2 (2010) 454–460, https://doi.org/10.1038/nchem.623.

[10] L. Bu, N. Zhang, S. Guo, X. Zhang, J. Li, J. Yao, T. Wu, G. Lu, J.-Y. Ma, D. Su, X. Huang, Biaxially strained PtPb/Pt core/shell nanoplate boosts oxygen reduction catalysis, Science 80 (354) (2016) 1410–1414.

[11] S. Rudi, L. Gan, C. Cui, M. Gliech, P. Strasser, Electrochemical dealloying of bimetallic ORR nanoparticle catalysts at constant electrode potentials, J. Electrochem. Soc. 162 (2015) F403–F409, https://doi.org/10.1149/2.0621504jes.

[12] J. Snyder, T. Fujita, M.W. Chen, J. Erlebacher, Oxygen reduction in nanoporous metal-ionic liquid composite electrocatalysts, Nat. Mater. 9 (2010) 904–907, https://doi.org/10.1038/nmat2878.

[13] J. Snyder, K. Livi, J. Erlebacher, Oxygen reduction reaction performance of [MTBD][beti]-encapsulated nanoporous NiPt alloy nanoparticles, Adv. Funct. Mater. 23 (2013) 5494–5501, https://doi.org/10.1002/adfm.201301144.

[14] J. Erlebacher, An atomistic description of dealloying, J. Electrochem. Soc. 151 (2004) C614, https://doi.org/10.1149/1.1784820.

[15] X. Li, Q. Chen, I. McCue, J. Snyder, P. Crozier, J. Erlebacher, K. Sieradzki, Dealloying of noble-metal alloy nanoparticles, Nano Lett. 14 (2014) 2569–2577, https://doi.org/10.1021/nl500377g.

[16] K.J.J. Mayrhofer, D. Strmcnik, B.B. Blizanac, V. Stamenkovic, M. Arenz, N. M. Markovic, Measurement of oxygen reduction activities via the rotating disc electrode method: from Pt model surfaces to carbon-supported high surface area catalysts, Electrochim. Acta. 53 (2008) 3181–3188, https://doi.org/10.1016/j.electacta.2007.11.057.

[17] M. Bele, M. Gatalo, P. Jovanovič, F. Ruiz-Zepeda, M. Šala, E. Šest, N. Hodnik, S. Hočevar, I. Gatto, A. Saccà, A.S. Aricò, M. Gaberšček, Insight on single cell proton exchange membrane fuel cell performance of Pt-Cu/C cathode, Catalysts 9 (2019) 544, https://doi.org/10.3390/catal9060544.

[18] L. Asen, G. Ercolano, F. Dionigi, S. Martens, C. Zalitis, A. Martinez, Comparison of Oxygen Reduction Reaction Measurements on Platinum Electrocatalysts Utilising Rotating Disk and Floating Electrodes with those from Membrane Electrode Assemblies, 162 (2015) 4329.

[19] S. Martens, L. Asen, G. Ercolano, F. Dionigi, C. Zalitis, A. Hawkins, A. Martinez Bonastre, L. Seidl, A.C. Knoll, J. Sharman, P. Strasser, D. Jones, O. Schneider, A comparison of rotating disc electrode, floating electrode technique and membrane electrode assembly measurements for catalyst testing, J. Power Sources. 392 (2018) 274–284, https://doi.org/10.1016/j.jpowsour.2018.04.084.

[20] S. Nösberger, J. Du, J. Quinson, E. Berner, A. Zana, G.K.H. Wiberg, M. Arenz, The gas diffusion electrode setup as a testing platform for evaluating fuel cell catalysts: a comparative RDE-GDE study, Electrochem. Sci. Adv. (2022), https://doi.org/10.1002/elsa.202100190.

[21] B. Han, C.E. Carlton, A. Kongkanand, R.S. Kukreja, B.R. Theobald, L. Gan, R. O'Malley, P. Strasser, F.T. Wagner, Y. Shao-Horn, Record activity and stability of dealloyed bimetallic catalysts for proton exchange membrane fuel cells, Energy Environ. Sci. 8 (2015) 258–266, https://doi.org/10.1039/c4ee02144d.

[22] I.E.L. Stephens, J. Rossmeisl, I. Chorkendorff, Toward sustainable fuel cells, Science 80 (354) (2016) 1378–1379, https://doi.org/10.1126/science.aal3303.

[23] R. Loukrakpam, B.F. Gomes, T. Kottakkat, C. Roth, A bird's eye perspective of the measurement of oxygen reduction reaction in gas diffusion electrode half-cell set-ups for pt electrocatalysts in acidic media, Jphys Mater. 4 (2021), https://doi.org/10.1088/2515-7639/ac0319.

[24] C.Y. Ahn, J.E. Park, S. Kim, O.H. Kim, W. Hwang, M. Her, S.Y. Kang, S. Park, O. J. Kwon, H.S. Park, Y.H. Cho, Y.E. Sung, Differences in the electrochemical performance of Pt-based catalysts used for polymer electrolyte membrane fuel cells in liquid half-and full-cells, Chem. Rev. 121 (2021), https://doi.org/10.1021/acs.chemrev.0c01337.

[25] A. Kongkanand, M.F. Mathias, The priority and challenge of high-power performance of low-platinum proton-exchange membrane fuel cells, J. Phys. Chem. Lett. 7 (2016) 1127–1137, https://doi.org/10.1021/acs.jpclett.6b00216.

[26] T. Lazaridis, B.M. Stühmeier, H.A. Gasteiger, H.A. El-Sayed, Capabilities and limitations of rotating disk electrodes versus membrane electrode assemblies in the investigation of electrocatalysts, Nat. Catal. 5 (2022) 363–373, https://doi.org/10.1038/s41929-022-00776-5.

[27] W. Zhou, X. Meng, L. Rajic, Y. Xue, S. Chen, Y. Ding, K. Kou, Y. Wang, J. Gao, Y. Qin, A.N. Alshawabkeh, "Floating" cathode for efficient H2O2 electrogeneration applied to degradation of ibuprofen as a model pollutant, Electrochem. Commun. 96 (2018) 37–41, https://doi.org/10.1016/j.elecom.2018.09.007.

[28] X. Lin, C.M. Zalitis, J. Sharman, A. Kucernak, Electrocatalyst performance at the gas/electrolyte interface under high-mass-transport conditions: optimization of the "floating electrode" method, ACS Appl. Mater. Interfaces. 12 (2020) 47467–47481, https://doi.org/10.1021/acsami.0c12718.

[29] Z. Long, Y. Li, G. Deng, C. Liu, J. Ge, S. Ma, W. Xing, Micro-membrane electrode assembly design to precisely measure the in situ activity of oxygen reduction reaction electrocatalysts for PEMFC, Anal. Chem. 89 (2017) 6309–6313, https://doi.org/10.1021/acs.analchem.7b01507.

[30] C. Zalitis, A. Kucernak, X. Lin, J. Sharman, Electrochemical Measurement of Intrinsic Oxygen Reduction Reaction Activity at High Current Densities as a Function of Particle Size for Pt 4–x Co x /C (x = 0, 1, 3) Catalysts, ACS Catal. 10 (2020) 4361–4376, https://doi.org/10.1021/acscatal.9b04750.

[31] C.M. Zalitis, D. Kramer, A.R. Kucernak, Electrocatalytic performance of fuel cell reactions at low catalyst loading and high mass transport, Phys. Chem. Chem. Phys. 15 (2013) 4329–4340, https://doi.org/10.1039/c3cp44431g.

[32] K. Ehelebe, N. Schmitt, G. Sievers, A.W. Jensen, A. Hrnjić, P. Collantes Jiménez, P. Kaiser, M. Geuß, Y.-P. Ku, P. Jovanovič, K.J.J. Mayrhofer, B. Etzold, N. Hodnik, M. Escudero-Escribano, M. Arenz, S. Cherevko, Benchmarking fuel cell electrocatalysts using gas diffusion electrodes: inter-lab comparison and best practices, ACS Energy Lett. 7 (2022) 816–826, https://doi.org/10.1021/acsenergylett.1c02659.

[33] A. Hrnjić, F. Ruiz-Zepeda, M. Gaberšček, M. Bele, L. Suhadolnik, N. Hodnik, P. Jovanovič, Modified floating electrode apparatus for advanced characterization of oxygen reduction reaction electrocatalysts, J. Electrochem. Soc. 167 (2020) 166501, https://doi.org/10.1149/1945-7111/abc9de.

[34] Product page of Pt-Fe/C from FCS: https://www.fuelcellstore.com/20-platinum-iron-vulcan, (n.d.).

[35] K.J.J. Mayrhofer, B.B. Blizanac, M. Arenz, V.R. Stamenkovic, P.N. Ross, N.M. Markovic, The Impact of Geometric and Surface Electronic Properties of Pt-Catalysts on the Particle Size Effect in Electrocatalysis, (2005) 14433–14440.

[36] V. Stamenkovié, M. Arenz, P.N. Ross, N.M. Markovié, Temperature-induced deposition method for anchoring metallic nanoparticles onto reflective substrates for in situ electrochemical infrared spectroscopy, J. Phys. Chem. b. 108 (2004) 17915–17920, https://doi.org/10.1021/jp0467301.

[37] M. Nesselberger, S. Ashton, J.C. Meier, I. Katsounaros, K.J.J. Mayrhofer, M. Arenz, The particle size effect on the oxygen reduction reaction activity of Pt catalysts: influence of electrolyte and relation to single crystal models, J. Am. Chem. Soc. 133 (2011) 17428–17433, https://doi.org/10.1021/ja207016u.

[38] L.J. Moriau, A. Hrnjić, A. Pavlišič, A.R. Kamšek, U. Petek, F. Ruiz-Zepeda, M. Šala, L. Pavko, V.S. Šelih, M. Bele, P. Jovanovič, M. Gatalo, N. Hodnik, Resolving the nanoparticles' structure-property relationships at the atomic level: a study of Pt-based electrocatalysts, Iscience. 24 (2021) 102102, https://doi.org/10.1016/j.isci.2021.102102.

[39] J. Greeley, I.E.L. Stephens, A.S. Bondarenko, T.P. Johansson, H.A. Hansen, T. F. Jaramillo, J. Rossmeisl, I. Chorkendorff, J.K. Nørskov, J. Greeley, I.E. L. Stephens, A.S. Bondarenko, T.P. Johansson, H.A. Hansen, T.F. Jaramillo, I. J. Rossmeis Chorkendorffl, J.K. Nørskov, J. Greeley, I.E.L. Stephens, A. S. Bondarenko, T.P. Johansson, H.A. Hansen, T.F. Jaramillo, J. Rossmeisl, I. Chorkendorff, J.K. Nørskov, Alloys of platinum and early transition metals as oxygen reduction electrocatalysts, Nat. Chem. 1 (2009) 552–556, https://doi.org/10.1038/nchem.367.

[40] V.R. Stamenkovic, B.S. Mun, K.J.J. Mayrhofer, P.N. Ross, N.M. Markovic, Effect of surface composition on electronic structure, stability, and electrocatalytic properties of Pt-transition metal alloys: Pt-Skin versus Pt-Skeleton Surfaces, J. Am. Chem. Soc. 128 (2006) 8813–8819, https://doi.org/10.1021/ja0600476.

[41] M. Oezaslan, F. Hasché, P. Strasser, Pt-based core–shell catalyst architectures for oxygen fuel cell electrodes, J. Phys. Chem. Lett. 4 (2013) 3273–3291, https://doi.org/10.1021/jz4014135.

[42] P. Strasser, S. Kühl, Dealloyed Pt-based core-shell oxygen reduction electrocatalysts, Nano Energy 29 (2016) 166–177, https://doi.org/10.1016/j.nanoen.2016.04.047.

[43] J. Mavrikakis, M. Hammer, B. Nørskov, M. Mavrikakis, B. Hammer, J.K. Nørskov, Effect of strain on the reactivity of metal surfaces, PhysRevLett. 81 (1998) 2819–2822, https://doi.org/10.1103/PhysRevLett.81.2819.

[44] M. Escudero-Escribano, P. Malacrida, M.H. Hansen, U.G. Vej-Hansen, A. Velázquez-Palenzuela, V. Tripkovic, J. Schiøtz, J. Rossmeisl, I.E.L. Stephens, I. Chorkendorff, Tuning the activity of Pt alloy electrocatalysts by means of the lanthanide contraction, Science 80 (352) (2016) 73–76, https://doi.org/10.1126/science.aad8892.

[45] J. Snyder, I. Mccue, K.J. Livi, J.D. Erlebacher, Structure/processing/properties relationships in nanoporous nanoparticles as applied to catalysis of the cathodic oxygen reduction reaction, J. Am. Chem. Soc. 134 (2012) 8633–8645, https://doi.org/10.1021/ja3019498.

[46] M. Escudero-Escribano, K.D. Jensen, A.W. Jensen, Recent advances in bimetallic electrocatalysts for oxygen reduction: design principles, structure-function relations and active phase elucidation, Curr. Opin. Electrochem. 8 (2018) 135–146, https://doi.org/10.1016/J.COELEC.2018.04.013.

[47] M. Oezaslan, M. Heggen, P. Strasser, Size-dependent morphology of dealloyed bimetallic catalysts : linking the nano to the macro scale, JACS. 134 (2012) 514–524.

[48] T.A. Greszler, D. Caulk, P. Sinha, J. Electrochem. Soc. 159 (2012) F831–F840, https://doi.org/10.1149/2.061212jes.

[49] A. Ohma, T. Mashio, K. Sato, H. Iden, Y. Ono, K. Sakai, K. Akizuki, S. Takaichi, K. Shinohara, Analysis of proton exchange membrane fuel cell catalyst layers for reduction of platinum loading at Nissan, Electrochim. Acta. 56 (2011) 10832–10841, https://doi.org/10.1016/j.electacta.2011.04.058.

[50] J.P.E.J.P.E. Owejan, J.P.E.J.P.E. Owejan, W. Gu, Impact of platinum loading and catalyst layer structure on PEMFC performance, J. Electrochem. Soc. 160 (2013) F824–F833, https://doi.org/10.1149/2.072308jes.

[51] M. Lopez-Haro, L. Guétaz, T. Printemps, A. Morin, S. Escribano, P.-H.-H. Jouneau, P. Bayle-Guillemaud, F. Chandezon, G. Gebel, Three-dimensional analysis of Nafion layers in fuel cell electrodes, Nat. Commun. 5 (2014) 1–6, https://doi.org/10.1038/ncomms6229.

[52] M. Lee, M. Uchida, H. Yano, D.A. Tryk, H. Uchida, M. Watanabe, New evaluation method for the effectiveness of platinum/carbon electrocatalysts under operating conditions, Electrochim. Acta. 55 (2010) 8504–8512, https://doi.org/10.1016/j.electacta.2010.07.071.

[53] M. Markiewicz, C. Zalitis, A. Kucernak, Performance measurements and modelling of the ORR on fuel cell electrocatalysts - The modified double trap model, Electrochim. Acta. 179 (2015) 126–136, https://doi.org/10.1016/j.electacta.2015.04.066.

[54] E. Benn, H. Uvegi, J. Erlebacher, Characterization of nanoporous metal-ionic liquid composites for the electrochemical oxygen reduction reaction, J. Electrochem. Soc. 162 (2015) H759–H766, https://doi.org/10.1149/2.0161510jes.